Solution of Time Dependent Joule Heat Equation for a Graphene Sheet Under Thomson Effect

Rekha Verma, *Student Member, IEEE,* Sitangshu Bhattacharya, *Member, IEEE,* and Santanu Mahapatra, *Senior Member, IEEE*

***Abstract*— We address a physics-based solution of joule heating phenomenon in a single-layer graphene (SLG) sheet under the presence of Thomson effect. We demonstrate that the temperature in an isotopically pure (containing only C^{12}) SLG sheet attains its saturation level quicker than when doped with its isotopes (C^{13}). From the solution of the joule heating equation, we find that the thermal time constant of the SLG sheet is in the order of tenths of a nanosecond for SLG dimensions of a few micrometers. These results have been formulated using the electron interactions with the inplane and flexural phonons to demonstrate a field-dependent Landauer transmission coefficient. We further develop an analytical model of the SLG specific heat using the quadratic (out of plane) phonon band structure over the room temperature. Additionally, we show that a cooling effect in the SLG sheet can be substantially enhanced with the addition of C^{13}. The methodologies as discussed in this paper can be put forward to analyze the graphene heat spreader theory.**

***Index Terms*— Electrothermal cooling, graphene, phonons.**

I. Introduction

THE electrothermal analyses of metallic graphene for next generation heat spreaders have gained momentum because of three reportedly vital reasons: 1) single-layer graphene (SLG) can withstand a very high room temperature (RT) breakdown current density of the order of 10^8-10^9 Acm^{-2} [1]–[3]; 2) it has an exceptionally high RT carrier mobility of the order of 20 000–20 0000 cm^{2}V^{-1}s^{-1} [4]; and 3) it possesses a phonon-dominated high RT thermal conductivity (κ) 600–7000 Wm^{-1}K^{-1} [1]. It is due to these exceptional properties that metallic graphene finds potential applications as chip interconnects [3], [5]–[6]. However, there also remain potential challenges to predict the extent of joule heating along the graphene itself to estimate the thermal propagation/delay [7].

Lately, there have been some remarkable experimental analyses (in both suspended and on-substrate SLG) on carrier mobility [8], electrical [9]–[13], and thermal [1], [14]–[17] (effects of C^{13} isotopes have been reported in [18]) resistances together with Peltier cooling [19]. These data can now be classified in terms of tension offered by the contacts to the SLG sheet. It now appeared that the involvement of out-of-plane (known as flexural) phonons can also play a substantial role, in case the sheet relaxes with the contacts at two ends [20], [21] and has been considered through rigorous molecular dynamic simulations and theory [21]–[24]. Following this, the authors [25] recently addressed an analytical model for an electrical resistance (R) through the solution of steady-state joule self-heating equation at different current levels considering a temperature-dependent thermal conductivity [26]. The motivation of this paper is sought out to estimate the transient analyses of the temperature over the SLG surface (under relaxed state with the contacts) when there is an applied temperature difference ΔT at the two ends apart from joule heating current. We start with the formulation of the Landauer field-dependent transmission coefficient ($\top(E)$) using the Mc Kelvey's carrier flux theory [27]. In such a case, the sheet resistance becomes a function of the applied field ε and local sheet temperature. With this and applied ΔT, the additional Thomson effect emerges where heat is either absorbed or rejected along the length of the sheet depending on direction of the current flow and sign of Seebeck coefficient (S_B), which in this case may conclude a profound cooling effect along the SLG sheet. Using a quadratic phonon band structure, we formulate a temperature-dependent flexural phonon specific heat $C_{\rm ph}$, to finally estimate the transient behavior of T. We also demonstrate the effect of including C^{13} isotopes on the same for optimization.

II. Modeling and Simulation Methodology

A. Average Energy of Electrons in SLG Sheet

Using the Dirac cone-type electron dispersion relation, the electron energy in SLG can be written as $E = \hbar v_F k$, in which $\hbar$, v_F ($=10^6$ ms^{-1}) and k are the reduced Planck's constant, Fermi velocity, and electron wave vector, respectively. Using this and considering the spin and valley degeneracies, the 2-D density of states can be written as $N_{2D}(E) = (2/\pi)\left(E/(\hbar v_F)^2\right)$. The average electron energy per sub-band can then be formulated from

$$\langle E_{2D}\rangle = \frac{\int_{E_\phi}^{\infty} N_{2D}(E)\,\mathrm{Ef}(E)\,\mathrm{dE}}{\int_{E_\phi}^{\infty} N_{2D}(E)\,f(E)\,\mathrm{dE}} \tag{1}$$

where E_ϕ is the lowest sub-band energy (in this case, this has a value zero at Dirac point) and $f(E)$ is the Fermi–Dirac occupation probability. Substituting the aforementioned values, (1) reads out $\langle E_{2D}\rangle = 2k_BT\,[F_2(\eta)/F_1(\eta)]$ in which k_B

Manuscript received April 15, 2013; revised July 18, 2013; accepted July 28, 2013. Date of publication August 19, 2013; date of current version September 18, 2013. The review of this paper was arranged by Editor R. Venkatasubramanian.

R. Verma and S. Mahapatra are with the nanoscale Device Research Laboratory, Department of Electronic Systems Engineering, Indian Institute of Science, Bangalore 560012, India (e-mail: rekha.verma26@gmail.com; santanu@cedt.iisc.ernet.in).

S. Bhattacharya is with the Department of Electrical Engineering, School of Engineering, Shiv Nadar University, Dadri 203207, India (e-mail: sitangshu.bhattacharya@snu.edu.in).

Color versions of one or more of the figures in this paper are available online at http://ieeexplore.ieee.org.

Digital Object Identifier 10.1109/TED.2013.2275896

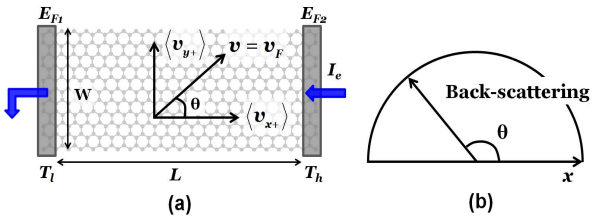

Fig. 1. (a) Schematic diagram of an SLG sheet of dimension $L \times W$. The contacts 1 and 2 are assumed to be ideal, long enough to avoid heat flow into the contacts and maintained at temperature T_l and T_h, respectively. The heat dissipation to the substrate is neglected by assuming a suspended condition. The electric current I_e is along the $-x$-direction. The Fermi energies are E_{F_1} and E_{F_2} at both the contacts with $E_{F_1} - E_{F_2} = \mathrm{qV}_D$. (b) Averaging of the backscattering length over the entire SLG sheet (2).

is the Boltzmann's constant, $F_j(\eta)$ is the Fermi–Dirac integral of order j and $\eta = E_F/k_BT$. Evidently, one can see that under nondegenerate carrier doping, $\langle E_{2D} \rangle \sim 2k_BT$ while for high doping, $\langle E_{2D} \rangle \sim (2/3)E_F$, where the Fermi energy with respect to the conduction band minimum can be written as $E_F = \hbar v_F \sqrt{n_{2D}\pi}$ in which n_{2D} is the 2-D electron density.

To evaluate the current flow through the SLG sheet, the evaluation of the number of channels is mandatory. As shown in Fig. 1(a), we consider an SLG of length L and width W. Due to the distribution of carrier velocity along both longitudinal as well as transverse direction, one has to consider the net average electron velocity along $+x$ direction, which is $\langle v_{x+} \rangle = (v_F/\pi)\int_{-\pi/2}^{+\pi/2} \cos\theta d\theta = (2/\pi)v_F$. This gives the number of channels as $M(E) = 2\mathrm{WE}/\pi\hbar v_F$.

B. Field-Dependent Electronic Transmission Coefficient in SLG Sheet

With the average velocity of the electrons along $+x$ direction, the energy-dependent net backscattering length, $\lambda_{2D}(x)$ is averaged over the entire length $+x$ to $-x$ [Fig. 1(b)] [28]. This gives the isotropic $\lambda_{2D}(x)$ as

$$\lambda_{2D}(x) = \frac{\pi}{2} v_F \tau_{e-p} \tag{2}$$

where $1/\tau_{e-p}$ is the resultant quasi-elastic electron–phonon (e-p) scattering rate because of interaction between the electrons and inplane and flexural phonons, which is given by Matthiessen's rule as $1/\tau_{e-p} = 1/\tau_{\text{inplane}} + 1/\tau_{\text{flexural}}$ where

$$\frac{1}{\tau_{\text{inplane}}} \approx \left[\frac{g^2}{2v_L^2} + \frac{\hbar^2 v_F^2 \beta^2}{4a^2}\left(\frac{1}{v_L^2} + \frac{1}{v_T^2}\right)\right] \frac{\langle E_{2D} \rangle}{2\rho\hbar^3 v_F^2} k_BT \tag{3}$$

and

$$\frac{1}{\tau_{\text{flexural}}} \approx \left(\frac{g^2}{2} + \frac{\hbar^2 v_F^2 \beta^2}{4a^2}\right) \frac{(k_BT)^2}{64\pi\hbar\varsigma^2 \langle E_{2D} \rangle} \ln\left(\frac{k_BT}{\hbar\omega_c}\right). \tag{4}$$

Here, $g \approx 3$ eV is the screened deformation potential constant, $\beta \approx 2-3$, $\varsigma = 1$ eV is the bending rigidity [24], $a = 1.4$ Å is the distance between the nearest carbon atoms, $\rho = 7.6 \times 10^{-7}$ Kgm^{-2} is the mass density, $v_L = 2.1 \times 10^4$ms^{-1} and $v_T = 1.4 \times 10^4$ ms^{-1} are the longitudinal and transverse sound velocities, respectively [24], ω_c is the infrared phonon cutoff frequency. In deriving (3) and (4), it has been assumed that the Bloch–Gruneisen temperature $\left(T_{\text{BG}} = 57(n_{2D})^{1/2}, 38(n_{2D})^{1/2}$ and $0.1(n_{2D}{}^{1/2})\right)$ K, in which n_{2D} is the order of 10^{16} m^{-2}) is far less than the RT for longitudinal, transverse, and flexural phonons, respectively, and the domination of the absorption or emission of two phonons for $T \gg T_{BG}$.

In the presence of a constant electric field ε along $-x$-direction, the electron gains energy by an amount $q\varepsilon x$ in addition to $\langle E_{2D} \rangle$. Hence, in such a case, using (3) and (4), (2) can be written as follows:

$$\lambda_{2D}(x) = \frac{\pi}{2} v_F \left[\frac{\langle E_{2D} \rangle + q\varepsilon x}{D + C\left(\langle E_{2D} \rangle + q\varepsilon x\right)^2}\right]. \tag{5}$$

Following Mc Kelvey's method [27], the net electron flux along $+x$-direction can then be written as

$$\frac{\mathrm{d}}{\mathrm{dx}}\left[n_{2D}^+(x)\langle v_{x+}\rangle\right] = \frac{-1}{\lambda_{2D}(x)}\left[n_{2D}^+(x) - n_{2D}^-(x)\right]\langle v_x \rangle \tag{6}$$

in which $n_{2D}^{\pm}(x)$ is the electron density along the $+$- and $-x$-directions, respectively and the average velocity $\langle v_x \rangle$ along both the x-directions are assumed to be the same. Using the current flow continuity equation

$$\left[n_{2D}^+(x) - n_{2D}^-(x)\right]\langle v_x \rangle = \left[n_{2D}^+(0) - n_{2D}^-(0)\right]\langle v_0 \rangle \tag{7}$$

and the boundary condition

$$n_{2D}^+(L)\langle v_{L+}\rangle = \left[n_{2D}^+(0) - n_{2D}^-(0)\right]\langle v_0 \rangle \tag{8}$$

$\top\left(\langle E_{2D} \rangle\right)$ can be evaluated as

$$\top\left(\langle E_{2D} \rangle\right) = 1 - \frac{n_{2D}^-(0)}{n_{2D}^+(0)} = \frac{1}{1+\phi} \tag{9}$$

where

$$\phi = \frac{2}{\pi v_F}\left\{\frac{D}{q\varepsilon} ln\left(1 + \frac{L}{L_{\text{kT}}}\right) + C\langle E_{2D} \rangle L\left(1 + \frac{L}{2L_{\text{kT}}}\right)\right\} \tag{10}$$

in which $L_{\text{kT}} = \langle E_{2D} \rangle / q\varepsilon$ and is generally denoted as the distance to which the potential drops to a value k_BT/q of its maximum at the source terminal, if the channel has a parabolic energy band structure and nondegenerate [27]. For the present case, this value lies between $2k_BT/q\varepsilon \le L_{\text{kT}} \le 2E_F/3q\varepsilon$. Evidently, in the low field limit, $L/L_{\text{kT}} \to 0$ which implies $\phi \to (2/(\pi v_F))\left[D/\langle E_{2D} \rangle + C\langle E_{2D} \rangle\right]L$ and thus, $\top\left(\langle E_{2D} \rangle\right) \to \lambda_{2D}/\lambda_{2D} + L$ where $\lambda_{2D} = (\pi/2)v_F\tau\left(\langle E_{2D} \rangle\right)$. Hence, we see that (9) can be well applied for both the regimes of carrier degeneracies.

C. ElectroThermal Currents in SLG Sheet

From Fig. 1 and using Landauer approach, the electric and electron heat currents under the application of small potential and temperature difference can be written as follows:

$$I_e = \frac{2q}{h}\int \top(E) M(E)\left[f_1(E) - f_2(E)\right]\mathrm{dE} \tag{11}$$

and

$$I_Q = \frac{2}{h}\int \left(E - E_{F_1}\right) \top(E) M(E)\left[f_1(E) - f_2(E)\right]\mathrm{dE}. \tag{12}$$

In such case, one can expand $f_2(E)$ using Taylor's method to give

$$f_2(E) = f_1(E) + \frac{\partial f_1(E)}{\partial E}\triangle E + \frac{\partial f_1(E)}{\partial T}\triangle T. \quad (13)$$

Using (13) in (11) and (12) gives the Onsager's relations

$$I_e = G\triangle V + S\triangle T \quad (14)$$

and

$$I_Q = -\mathrm{TS}\triangle V - K_e\triangle T \quad (15)$$

where

$$G = \frac{2q^2}{h}\int \top(E) M(E)\left[-\frac{\partial f_1(E)}{\partial E}\right]\mathrm{dE} \quad (16)$$

is the electrical conductance,

$$S = \frac{-2q}{h}\int \top(E) M(E)\left(\frac{E-E_{F_1}}{T}\right)\left[-\frac{\partial f_1(E)}{\partial E}\right]\mathrm{dE} \quad (17)$$

is the Soret coefficient, and

$$K_e = \frac{2}{h}\int \top(E) M(E)\left(E-E_{F_1}\right)^2\frac{1}{T}\left[-\frac{\partial f_1(E)}{\partial E}\right]\mathrm{dE} \quad (18)$$

is the short-circuit electron-dominated thermal conductance. At this point, it should clearly be understood that $\top(E)$ in (12) and hence in (17) and (18) are to be found out when there is no applied electric field. Following Fig. 1(a), and assuming a uniform carrier (or doping) density, (14) and (15) can be written in terms of current densities along $-x$-directions as

$$J_e = \sigma\left(\frac{\partial V}{\partial x}\right) - \frac{S}{W}\left(\frac{\partial T}{\partial x}\right) \quad (19)$$

$$J_Q = -\frac{\mathrm{TS}}{W}\left(\frac{\partial V}{\partial x}\right) - \frac{K_e + K_{\mathrm{ph}}}{W}\left(\frac{\partial T}{\partial x}\right) \quad (20)$$

where the heat flow because of phonons is also added to (20). As the thermal conductance in SLG is mainly dominated by phonons [1], [14]–[17], [21]–[25], [26], one can fairly take $K_{\mathrm{ph}} \gg K_e$. Thus, from (19), we can write

$$J_Q = \mathrm{TS}_B J_e - \left(\kappa_{\mathrm{ph}}(T) - \frac{\mathrm{TS}_B^2 G}{W}\right)\left(\frac{\partial T}{\partial x}\right) \quad (21)$$

where $S_B\,(=S/G)$ is the Seebeck coefficient and $\kappa_{\mathrm{ph}}(T)$ is the phonon thermal conductivity. Using the degenerate Mott relation, one can also rewrite $S_B = (\pi^2 k_B^2 T/3q)\left|1/G\,(\partial G/\partial E)\right|_{\varepsilon=0, E=\langle E_{2D}\rangle}$. At high carrier concentration, one can approximate the function $(\partial f_1/\partial E) = -\delta\left(E-E_{F_1}\right)$ and can carefully differentiate this to obtain

$$S_B = \frac{\pi^2 k_B^2 T}{3q}\left[\frac{\top'\left(E_{F_1}\right)}{\top\left(E_{F_1}\right)} + \frac{M'\left(E_{F_1}\right)}{M\left(E_{F_1}\right)}\right] \quad (22)$$

where $\top'\left(E_{F_1}\right)/\top\left(E_{F_1}\right) = (4L/3\pi\upsilon_F)\top\left(E_{F_1}\right)\left[9D/4E_{F_1}^2 - C\right]$ and $M'\left(E_{F_1}\right)/M\left(E_{F_1}\right) = 1/E_{F_1}$ and the primes denotes the differentiation with respect to the Fermi energy. As the temperature increases, $D \gg C$ and thus S_B tends to a dimension-independent value $5\pi^2 k_B^2 T/6qE_{F_1}$.

D. Specific Heat of SLG Sheet and Transient Joule Heating Equation

It was pointed out in [29] that the analyses of specific heat at low temperature signify the dimensionality of the system. This implies that at low temperature ($T \ll \Theta_D$, Θ_D is the Debye temperature of graphene) and considering a linear phonon dispersion relation, the contribution from the inplane phonons should exhibit a T^2 dependency. However, following the discussions in the Introduction, the specific heat contributed only by the ZA mode can be written from

$$C_{\mathrm{ph}} = \int_0^{\omega_{\max}}\left(\frac{\hbar\omega}{k_B T}\right)^2\frac{e^x}{(e^x-1)^2}\rho(\omega)\,d\omega \quad (23)$$

where $x = \hbar\omega/k_B T$, $\rho(\omega) = A/(2\pi)^2(2\pi K/(\partial\omega/\partial K))$ is the 2-D phonon density of states, which can be written as $\rho(\omega) = A/4\pi\alpha$ through the ZA mode phonon dispersion relation $\omega = \alpha K^2$ in which α is the ZA phonon diffusion constant (4.6×10^{-7} $\mathrm{m^2 s^{-1}}$) and K is the phonon wave vector. The parameter $A = ((3\sqrt{3})/4)r_0^2 N_A$ is the molar area with r_0 ($=0.14$ nm) is the carbon–carbon distance and N_A is the Avogadro's number per mole. In this case, for simplified solutions, we assume the classical phonon dynamics to obtain the ZA plane $\Theta_D = 1000$ K [30]. It can be seen from (23) that the analytical answer occurs only at $T \to \infty$ where the integrand $x^2e^x/(e^x-1)^2 \to 1$. In such a case, $C_{ph} \to \left[k_B^2\pi A/(2\pi)^2\alpha\hbar\right]\Theta_D$, a constant value as anticipated. However, at low temperatures, $C_{\mathrm{ph}} \to \left[k_B^2\pi A/(2\pi)^2\alpha\hbar\right]T\int_0^\infty x^2e^x/(e^x-1)^2\mathrm{dx}$. The parenthesis term is a constant and hence, C_{ph} follows a linear T behavior. It should be particularly understood that as the focus of this paper lies at the moderate temperature (300–500 K), it will lead to erroneous result in predicting the transient temperature distribution if one assumes either a constant or linear T dependency. To reduce the mathematical complexity arising from an integro-differential equation [using (23) in (25)], we use a fitting solution for C_{ph} as

$$C_{\mathrm{ph}} = \left[\frac{\pi \mathrm{A}k_B^2}{(2\pi)^2\alpha\hbar}\right]T\left[\left(\frac{\pi^2}{5.3927}\right)^2\tanh\left(\frac{3\Theta_D}{10T}\right)\right] \quad (24)$$

to corelate (23) over all the temperatures. Fig. 2 shows this variation with temperature over all the ranges, computed numerically. We see that at lower temperature, C_{ph} exhibits a linear T dependency while at higher T, tends to constant. The inset shows the nonlinear variation of C_{ph} above RT, which has been compared (open circles) with (24).

Thus, the transient Joule heating equation can then be written using (21) and the energy conservation law as

$$\frac{\partial}{\partial x}\left(\kappa_0\frac{\partial T}{\partial x}\right) - (\sigma\varepsilon S_B)\left(\frac{\partial T}{\partial x}\right) + \left(\frac{q\sigma S_B\varepsilon^2}{E_{F_1}}\right)T + \sigma\varepsilon^2 = \rho_v C_{\mathrm{ph}}\frac{\partial T}{\partial t} \quad (25)$$

where $\kappa_0 = \kappa_{\mathrm{ph}}(T) - \mathrm{TS}_B^2 G/W$, $\rho_v\left(=2.8\times10^3\ \mathrm{Kgm^{-3}}\right)$ is the volume density and σ is the SLG electrical conductivity. It is realizable from (25) that the first and last terms resemble Fourier's heat diffusion and Joule heating, respectively. However, the second and third terms came because of the evaluation

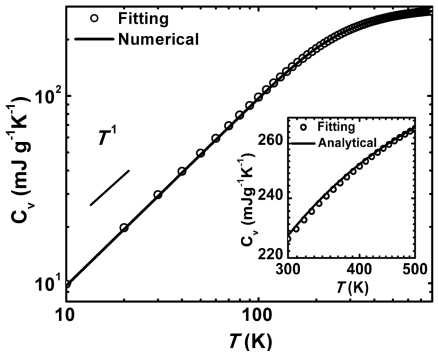

Fig. 2. Phonon specific heat as a function of T in SLG sheet. Lines: the numerical solution to (23). Symbols: the fitting equation (24). At lower temperature, C_{ph} is proportional to T. The inset magnifies the variation between 300–500 K.

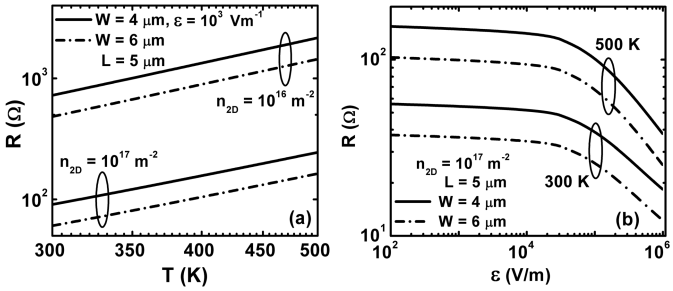

Fig. 3. (a) R as a function of T with varying sheet carrier concentration. (b) R as a function of å at different temperatures.

of $\partial S_B/\partial T$ from (22) by considering $D \gg C$. Furthermore, the evaluation of S_B from (25) leads to serious effects on the degree of rise in temperature over the n-doped SLG sheet as discussed in the following section.

At this point, it is also worth mentioning about contribution in κ_{ph} by ZA phonon in SLG sheet. Balandin *et al.* [1], [31]–[34] predicted a large κ_{ph} because of the high mean free path of the long wavelength phonons. However, the effect of ZA phonons was also exhibited in [21] and [22] using their numerical solution to the linearized phonon Boltzmann's transport equation and Lennard–Jones potential, respectively, and predicted that about 60% of the Umklapp and normal processes involving ZA mode are forbidden, causing a significant increase of κ_{ph}. Further, Alofi, *et al.* [35] predicted that κ_{ph} contribution from ZA branch is $\sim$2.1 times larger than from LA modes and $\sim$1.8 times that that of TA modes. However, if the sheet is on substrate/supported, LA/TA remains immune to substrate interactions but ZA modes are suppressed by phonon leakage through the substrate and is further studied by molecular dynamics simulations and Boltzmann's technique [36], [37]. Whatsoever, for suspended SLG sheet, [26] has demonstrated, using a second-order three-phonon Umklapp, the edge roughness, and isotopic scatterings, the variation of κ_{ph} with geometry, temperature, and isotope concentration that agrees well with the experiments cited there in. Considering this, it has been found that κ_{ph} follows a $T^{1.5}$ and T^{-2} law at lower and higher temperatures in the absence of isotopes, respectively [27]. However, in their presence, the behavior of κ_{ph} sharply deviates from the T^{-2} law at higher temperatures. To solve (25), we use analytical model of κ_{ph} from [26] in the following section.

III. Results and Discussions

Using the Landauer's conductance (16) and assuming a high n-type carrier concentration, the sheet resistance under uniform temperature distribution and electric field can be written as $R(T) = \left(h/2q^2\right)(1/\top(\langle E_{2D}\rangle)\, M(E_F))$. Fig. 3(a) shows this variation as a function of the sheet temperature under different carrier concentrations. It appears that the sheet resistance exhibits a linear variation with temperature when plotted in logarithmic scale. It can also be seen that with the increase in the sheet concentration, the resistance seems to fall because of the reason of increased Fermi energy, which increases the number of channels and decreases the transmission coefficient. The main scattering mechanism that dominates at higher temperature comes from the inplane interactions (6), which increases with the increase in the carrier concentration. This consequently increases the electron average energy, thereby increasing the scattering rate. Fig. 3(b) shows the variation of R as a function of electric field at different uniform sheet temperatures and widths. It can be understood that the resistance increases with L whereas with the increase in the width, R falls because of the increase in the number of channels. The effect of increase in electric field on the resistance exhibits a decrease in the variation of R. Clearly, this is due to the reduction of the backscattering length, which aids to transmit the carriers from contact 1 to 2. It should be noted that, currently, the role of ZO optical phonon emission at very high temperature and electric field ($\gg 10^6$ Vm^{-1}) is not clear hence, our theoretical results at that regime should be modeled carefully. However, as the field and temperature deviations (from 300 K) are less [see Taylor's expression (17)], the present analyses exhibit a reasonable physical insight.

To keep our presentation brief, we do not intend to exhibit the variation of R and S_B as the functions of sheet concentration and temperature. This has been already exhibited in [38], which is in good agreement with the experimental data mentioned there in. However, the notable conclusions from [38] are that S_B at RT decreases with the increase in n_{2D}.

In the presence of thermal current, the Thomson effect appears that depending on the direction of the field and type of carrier concentration may result in a heating or cooling along the sheet length. From (25), one can see the effect of the Seebeck coefficient S_B, which is negative for an n-type SLG, in the second and third terms. This results in a lowering of the temperature as time increases, far from the hot end, signifying a local cooling region instead of hot spot. A local heating occurs when either the direction of the thermal current or the electric current is changed or if we change the type of carrier concentration. As shown in Fig. 1(a), the electric and thermal currents are flowing in the same direction (right to left) hence absorbing the heat from the sheet, results in Thomson cooling and is shown in Fig. 4(a). It can be seen from this figure that with an increase in ε, the steady-state temperature goes down and reaches to a value of almost 292 K

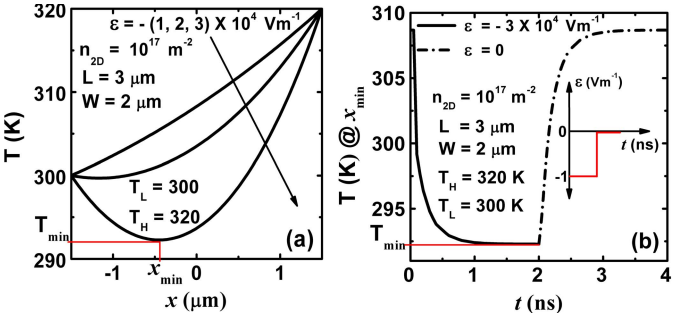

Fig. 4. (a) Static temperature profile along the sheet length with varying ε, directed from right to left [Fig. 1(a)]. (b) Transient behavior of the minimum temperature of the SLG at the cold- pot [$x = x_{\min}$ from solution of (25)] when $\varepsilon = -3 \times 10^4$ Vm^{-1} in the form of step input is applied across the sheet (directed from right to left as before) in the absence of any isotopes. The carriers are assumed to have sufficient relaxation time before flipping of the applied field.

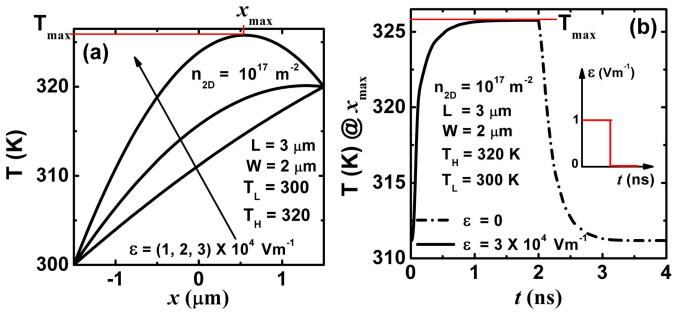

Fig. 5. Static temperature profile along the sheet length considering all respective cases of Fig. 4(a) and (b) with ε, directed from left to right [Fig. 1(a)].

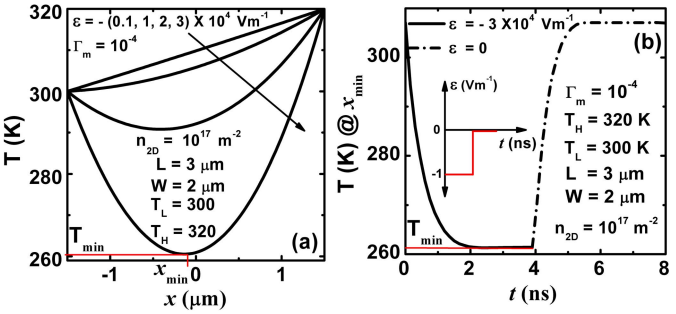

Fig. 6. (a) Static temperature profile along the sheet length with varying ε and is directed from right to left in the presence of C^{13} with $\Gamma_m = 10^{-4}$ (strength of the isotopic scattering). (b) Transient behavior of the minimum temperature at the cold spot [$x = x_{\min}$ from solution of (25)] when $\varepsilon = -3 \times 10^4$ Vm^{-1} in the form of step input is applied across the sheet.

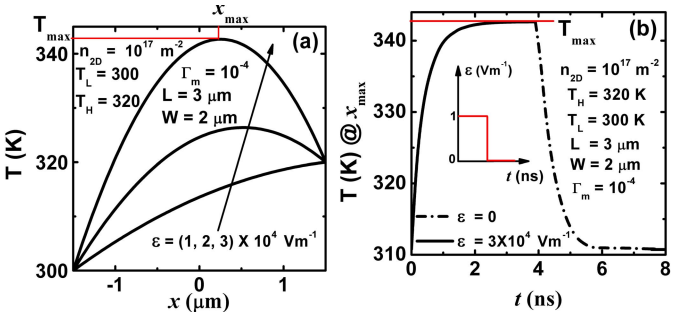

Fig. 7. Static temperature profile along the sheet length considering all respective cases of Fig. 6(a) and (b) with ε, directed from left to right [Fig. 1(a)].

from its initial value for a sheet dimension of 3×2 μm^2. Fig. 4(b) shows the temperature variation when a step input is applied. It appears that in the absence of isotopes, the minimum steady-state temperature is attained very quickly with a rise time (t_r) of almost 0.36 ns for the given dimensions. The fall time (t_f) is approximately 0.40 ns and reaches to the local initial temperature (when the field is removed). Fig. 5(a) and (b) shows just the opposite scenario of Fig. 4(a) and (b), respectively, i.e., an ε is applied in the opposite direction (left to right) and thermal current is flowing from right to left results in rejection of heat to the sheet ,and hence temperature along the length goes up and can reach up to a value of about 326 K with $\varepsilon = 3 \times 10^4$ Vm^{-1} for the given sheet dimensions. In this case, $t_r = 0.30$ ns while $t_f = 0.46$ ns, being much quicker. We thus observe from Figs. 4(b) and 5(b) that in the absence of any isotopes, the SLG sheet cools down and heats up, respectively, faster which is due to the involvement of the coefficient $\sigma \varepsilon S_B$ in the second term of (25).

Figs. 6(a) shows the static temperature profile along the sheet length for varying ε in the presence of C^{13} isotopes. It can be seen that the effect of addition of C^{13} isotopes lowers down the local temperature much, compared with that in the absence of isotopes [Fig. 4(a)]. With an increase in ε, T reduces and reaches to a value of about 261 K quite lower than the corresponding case of isotopically pure sheet. This is due to the increase of the isotopic phonon scattering rate, which decreases the thermal conductivity and effectively decreases κ_0. This consequently reduces the Fourier conduction term in (25). Fig. 6(b) shows the temperature rise when a step input is applied. It appears that the steady-state minimum temperature is attained in almost 1 ns, which is approximately 2.7 times than that of corresponding pure case for the same given dimensions, field and initial, and boundary conditions. It appeared that when the field is removed, t_f becomes 0.80 ns, which implies that under the presence of isotopes, the SLG sheet takes much longer time to reach the initial steady-state temperature. Fig. 7(a) and (b) shows all the cases of Fig. 5(a) and (b) under the presence of isotopes. It can be seen from Fig. 7(a) that under joule heating [electric field directed from left to right, Fig. 1(a)], an increase in ε increases the temperature. This can be compared with Fig. 5(a), which shows that the maximum temperature at $\Gamma_m = 10^{-4}$ can reach up to 342 K because of the above-mentioned reason. The rise and fall times are 0.92 and 0.97 ns, respectively, much larger that the identical cases of an isotopically pure SLG sheet.

At this point, it should be noted that this paper focusses only on the ZA contribution of the carrier transport properties of suspended SLG sheet. Our present $\top(E)$ methodology can also be used to predict the sheet temperature by considering the contribution from other acoustic phonon branches. For example, the contribution from the LA and TA phonon branches can increase the C_{ph} to almost 2–3 times than only ZA branch. In such a case, C_{ph}=700 JKg^{-1}K^{-1} at RT [39]. In case, the SLG is on substrate, the heat loss into the same must also be considered. Additionally, for short channel

length, the effect of contact resistances should be included which may have a profound change in the determination of overall G and thermal conductance. The theoretical analyses of our work estimate that isotopically doped suspended SLG sheet takes longer time to heat and cool, however, at the cost of magnitude of the temperature rise. The time constant in such case is in the order of a few nanoseconds and can be calculated from $\tau = R_{\text{th}} C_{\text{th}}/8$, where $R_{\text{th}} = L/\left(\kappa_{\text{ph}}(T)\, W\delta\right)$ is the thermal resistance and $C_{\text{th}} = (\text{LW}\delta)\,\rho_v C_{\text{ph}}(T)$ is the thermal capacitance [39]. This leads to about 0.16 ns at 300 K considering $\kappa_{\text{ph}} = 2500\ \text{Wm}^{-1}\text{K}^{-1}$ in the absence of any isotopes for the given dimensions [Fig. 5(b)].

IV. Conclusion

We estimate the transient response of temperature over a suspended SLG sheet under the presence of both electrical and thermal currents by formulating Landauer transmission coefficient and solution of joule heating equation. We find that for ZA phonon dominated SLG sheet, it takes longer time to cool/heat when isotopes are present.

Acknowledgement

The authors would like to acknowledge Prof. E. PoP at Department of Electrical Engineering, Stanford University (previously at UIUC), USA for valuable discussions.

References

[1] A. A. Balandin, "Thermal properties of graphene and nanostructured carbon materials," *Nature Mat.*, vol. 10, pp. 569–581, Jul. 2011.

[2] J. Yu, G. Liu, A. V. Sumant, V. Goyal, and A. A. Balandin, "Graphene-on-diamond devices with increased current-carrying capacity: Carbon sp^2-on-sp^3 technology," *Nano Lett.*, vol. 12, no. 3, pp. 1603–1608, Feb. 2012.

[3] (2012). *International Technology Roadmap for Semiconductors* [Online]. Available: http://www.itrs.net/Links/2009ITRS/2009Chapters 2009Tables/2009Interconnect.pdf

[4] S. V. Morozov, K. S. Novoselov, M. I. Katsnelson, F. Schedin, D. C. Elias, J. A. Jaszczak, and A. K. Geim, "Giant intrinsic carrier mobilities in graphene and its bilayer," *Phys. Rev. Lett.*, vol. 100, no. 1, pp. 016602-1–016602-4, Jan. 2008.

[5] D. Sarkar, C. Xu, H. Li, and K. Banerjee, "High-frequency behavior of graphene-based interconnects—Part I: Impedance modeling," *IEEE Trans. Electron Devices*, vol. 58, no. 3, pp. 843–852, Mar. 2011.

[6] A. Behnam, A. S. Lyons, M.-H. Bae, E. K. Chow, S. Islam, C. M. Neumann, and E. Pop, "Transport in nanoribbon interconnects obtained from graphene grown by chemical vapor deposition," *Nano Lett.*, vol. 12, no. 9, pp. 4424–4430, Aug. 2012.

[7] S. Islam, Z. Li, V. E. Dorgan, M.-H. Bae, and E. Pop, "Role of joule heating on current saturation and transient behavior of graphene transistors," *IEEE Electron Device Lett.*, vol. 34, no. 2, pp. 166–168, Feb. 2013.

[8] E. V. Castro, H. Ochoa, M. I. Katsnelson, R. V. Gorbachev, D. C. Elias, K. S. Novoselov, A. K. Geim, and F. Guinea, "Limits on charge carrier mobility in suspended graphene due to flexural phonons," *Phys. Rev. Lett.*, vol. 105, no. 26, pp. 266601-1–266601-4, Dec. 2010.

[9] K. I. Bolotin, K. J. Sikes, J. Hone, H. L. Stormer, and P. Kim, "Temperature-dependent transport in suspended graphene," *Phys. Rev. Lett.*, vol. 101, no. 9, pp. 096802-1–096802-4, Aug. 2008.

[10] Q. Shao, G. Liu, D. Teweldebrhan, and A. A. Balandin, "High-temperature quenching of electrical resistance in graphene interconnects," *Appl. Phys. Lett.*, vol. 92, no. 20, pp. 202108-1–202108-3, May 2008.

[11] F. T. Vasko and V. Ryzhii, "Voltage and temperature dependencies of conductivity in gated graphene," *Phys. Rev. B*, vol. 76, no. 23, pp. 233404-1–233404-4, Dec. 2007.

[12] A. D. Liao, J. Z. Wu, X. Wang, K. Tahy, D. Jena, H. Dai, and E. Pop, "Thermally limited current carrying ability of graphene nanoribbons," *Phys. Rev. B*, vol. 106, no. 25, pp. 256801-1–256801-4, Jun. 2011.

[13] D. K. Efetov and P. Kim, "Controlling electron-phonon interactions in graphene at ultrahigh carrier densities," *Phys. Rev. Lett.*, vol. 105, no. 25, pp. 256805-1–256805-4, Dec. 2010.

[14] E. Muñoz , J. Lu, and B. I. Yakobson,"Ballistic thermal conductance of graphene ribbons," *Nano Lett.*, vol. 10, no. 5, pp. 1652–1656, Apr. 2010.

[15] X. Xu, Y. Wang, K. Zhang, X. Zhao, S. Bae, M. Heinrich, C. T. Bui, R. Xie, J. T. L. Thong, B. H. Hong, K. P. Loh, B. Li, and B. Ozyilmaz, *Phonon Transport in Suspended Single Layer Graphene*. Ithaca, NY, USA: Cornell Univ. Press, 2010, pp. 1-4.

[16] Z.-Y. Ong and E. Pop, "Effect of substrate modes on thermal transport in supported graphene," *Phys. Rev. B*, vol. 84, no. 7, pp. 075471-1–075471-7, Aug. 2011.

[17] M. T. Pettes, I. Jo, Z. Yao, and L. Shi, "Influence of polymeric residue on the thermal conductivity of suspended bi-layer graphene," *Nano Lett.*, vol. 11, no. 3, pp. 1195–1200, Feb. 2011.

[18] S. Chen, Q. Wu, C. Mishra, J. Kang, H. Zhang, K. Cho, W. Cai, A. A. Balandin, and R. S. Ruoff, "Thermal conductivity of isotopically modified graphene," *Nature Mater.*, vol. 11, no. 3, pp. 203–207, Jan. 2012.

[19] K. L. Grosse, M.-H. Bae, F. Lian, E. Pop, and W. P. King, "Nanoscale Joule heating, Peltier cooling and current crowding at graphene–metal contacts," *Nature Nanotechnol.*, vol. 6, no. 5, pp. 287–290, Apr. 2011.

[20] S. D. Sarma and E. H. Hwang, "Density-dependent electrical conductivity in suspended graphene: Approaching the Dirac point in transport," *Phys. Rev. B*, vol. 87, pp. 035415-1–035415-13, Jan. 2013.

[21] E. Mariani and F von Oppen, "Flexural phonons in free-standing graphene," *Phys. Rev. Lett.*, vol. 100, no. 7, pp. 113401-1–113401-4, Feb. 2008.

[22] L. Lindsay, D. A. Broido, and N. Mingo, "Flexural phonons and thermal transport in graphene," *Phys. Rev. B*, vol. 82, no. 11, pp. 115427-1–115427-6, Sep. 2010.

[23] L. Lindsay, D. A. Broido, and N. Mingo, "Flexural phonons and thermal transport in multilayer graphene and graphite," *Phys. Rev. B*, vol. 83, no. 23, pp. 235428-1–235428-5, Jun. 2011.

[24] H. Ochoa, E. V. Castro, M. I. Katsnelson, and F. Guinea, "Scattering by flexural phonons in suspended graphene under back-gate induced strain," *Phys. E*, vol. 44, pp. 963–966, Sep. 2012.

[25] R. Verma, S. Bhattacharya, and S. Mahapatra, "Physics-based solution for electrical resistance of graphene under self-heating effect," *IEEE Trans. Electron Devices*, vol. 60, no. 1, pp. 502–505, Jan. 2013.

[26] R. Verma, S. Bhattacharya, and S. Mahapatra, "A physics based flexural phonon dependent thermal conductivity model for single layer graphene," *Semicond. Sci. Technol.*, vol. 28, no. 1, pp. 015009-1–015009-6, Jan. 2013.

[27] J. P. Mckelvey, R. L. Longini, and T. P. Brody, "Alternative approach to the solution of added carrier transport problems in semiconductors," *Phys. Rev.*, vol. 123, no. 1, pp. 51–57, Jul. 1961.

[28] C. Jeong, R. Kim, M. Luisier, S. Datta, and M. Lundstrom, "On Landauer versus Boltzmann and full band versus effective mass evaluation of thermoelectric transport coefficients," *J. Appl. Phys.*, vol. 107, pp. 023707-1–023707-7, Jan. 2010.

[29] J. Hone, "Phonons and thermal properties of carbon nanotubes," *Topics Appl. Phys.*, vol. 80, pp. 273–286, Aug. 2001.

[30] M. M. Sadeghi, M. T. Pettes, and L. Shi, "Thermal transport in graphene," *Solid State Commun.*, vol. 152, no. 15, pp. 1321–1330, Aug. 2012.

[31] D. L. Nika, E. P. Pokatilov, A. S. Askerov, and A. A. Balandin "Phonon thermal conduction in graphene: Role of Umklapp and edge roughness scattering," *Phys. Rev. B*, vol. 79, no. 15, pp. 155413-1–155413-12, Apr. 2009.

[32] D. L. Nika and A. A. Balandin, "Two-dimensional phonon transport in graphene," *J. Phys., Condensed Matter*, vol. 24, no. 23, pp. 233203-1–233203-18, Jun. 2012.

[33] D. L. Nika, A. S. Askerov, and A. A. Balandin, "Anomalous size dependence of the thermal conductivity of graphene ribbons," *Nano Lett.*, vol. 12, no. 6, pp. 3238–3244, 2012.

[34] D. L. Nika and A. A. Balandin, "Theoretical description of thermal transport in graphene: The issues of phonon cut-off frequencies and polarization branches," *Phys. status solidi (B)*, vol. 248, no. 11, pp. 2609–2614, Nov. 2011.

[35] A. Alofi and G. P. Srivastava, "Thermal conductivity of graphene and graphite," *Phys. Rev. B*, vol. 87, no. 11, pp. 115421-1–115421-10, Mar. 2013.

[36] Z. Aksamija and I. Knezevic, "Thermal transport in graphene nanoribbons supported on SiO_2," *Phys. Rev. B*, vol. 86, no. 16, pp. 165426-1–165426-6, 2012.

[37] L. Chen and S. Kumar, "Thermal transport in graphene supported on copper," *J. Appl. Phys.*, vol. 112, no. 4, pp. 043502-1–043502-7, Aug. 2012.

[38] R. Verma, S. Bhattacharya, and S. Mahapatra, "Thermoelectric performance of single layer graphene sheet for energy harvesting," *IEEE Trans. Electron Devices*, vol. 60, no. 6, pp. 2604–2070, Jun. 2013.

[39] E. Pop, (Feb. 2013). private communication.

Rekha Verma (S'12) is currently pursuing the Ph.D. degree in electrothermal transport in 1-D and 2-D layered materials for applications in interconnects and thermoelectric devices from the Department of Electronic Systems Engineering, Indian Institute of Science, Bangalore, India.

Sitangshu Bhattacharya (M'13) received the Ph.D. degree from Jadavpur University, Kolkata, India, in 2009.

He is currently a DST Inspire Faculty Member and an Assistant Professor with Shiv Nadar University, Dadri, India.

Santanu Mahapatra (M'08–SM'10) received the Ph.D. degree in electrical engineering from the École Polytechnique Fédrale de Lausanne, Lausanne, Switzerland, in 2005.

He is currently an Associate Professor with the Indian Institute of Science, Bangalore, India.